An Isosymmetric High-Pressure Phase Transition in α-Glycylglycine: A Combined Experimental and Theoretical Study

Samantha M. Clarke,*,[†] Brad A. Steele,*,[†] Matthew P. Kroonblawd,[†] Dongzhou Zhang,[‡] I-Feng W. Kuo,[†] and Elissaios Stavrou[†]

[†]Physical and Life Sciences Directorate, Lawrence Livermore National Laboratory, P.O. Box 808, Livermore, California 94550, United States

[‡]Partnership for Extreme Crystallography, University of Hawaii at Manoa, Argonne, Illinois 60439, United States

Ⓢ *Supporting Information*

ABSTRACT: We investigated the effects of hydrostatic pressure on α-glycylglycine (α-digly) using a combined experimental and theoretical approach. The results of powder X-ray diffraction show a change in compressibility of the axes above 6.7 GPa, but also indicate that the structure remains in the same monoclinic space group, suggesting an isosymmetric phase transition. A noticeable change in the Raman spectra between 6 and 7.5 GPa further supports the observed phase transition. First-principles-based calculations combined with the crystal structure prediction code USPEX predict a number of possible polymorphs at high pressure. An orthorhombic structure with a bent peptide backbone is the lowest enthalpy polymorph above 6.4 GPa; however, it is not consistent with experimental observations. A second monoclinic structure isosymmetric to α-digly, α′-digly, is predicted to become more stable above 11.4 GPa. The partial atomic charges in α′-digly differ from α-digly, and the molecule is bent, possibly indicating different reactivity of α′-digly. The similarity in the lattice parameters predicted from calculations and the axial changes observed experimentally support that the α′-digly phase is likely observed at high pressure. A possible explanation for the isosymmetric phase transition is discussed in terms of relaxing strained hydrogen bonding interactions. Such combined experimental and modeling efforts provide atomic-level insight into how pressure-driven conformational changes alter hydrogen-bonding networks in complicated molecular crystals.
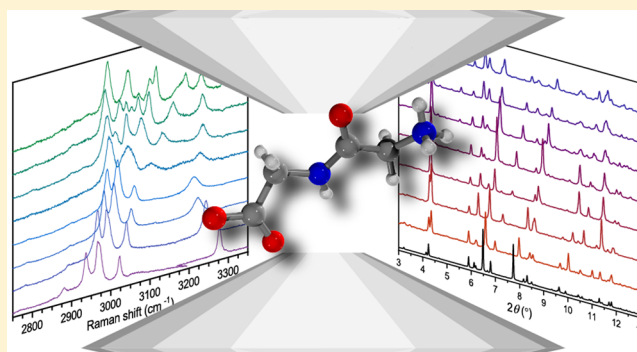
■ INTRODUCTION

Pressure is one of the fundamental physical variables that can affect stability, induce phase transitions, and/or promote oligomerization of biologically relevant molecules such as amino acids. Understanding the high-pressure behavior of amino acids is of practical importance for applications in the pharmaceutical and food industries[1] and is also fundamental to a number of theories on the origins of life. There is mounting evidence that moderate pressures in the kPa and MPa regimes, such as at hydrothermal vents, play a key role in promoting the oligomerization of amino acids.[2−6] Substantially higher GPa range pressures reached in impacting cometary ices could plausibly lead to the synthesis[7,8] and oligomerization[9−11] of amino acids and to the formation of complex polyaromatic molecules.[12] These hypotheses have sparked a number of efforts to understand the role of pressure on the equations of state (EOS) and crystal structures of simple amino acids.[10,11,13−21] However, developing a detailed understanding of pressure as a thermodynamic driver for the formation of larger biological precursors requires similar information for the products of amino acid oligomerization reactions, with the simplest case being dipeptides formed through condensation reactions.

Glycine ($C_2H_5NO_2$) is the simplest amino acid and has been studied at pressure extensively due to its importance as a model system in many origins of life scenarios.[16,17,20,22,23] The product of the condensation reaction between two glycine monomers is water and the simplest polypeptide, glycylglycine (herein termed digly), which contains just one achiral peptide bond.[24,25] In comparison, digly has been studied much less extensively at high pressures. At ambient conditions, it exhibits rich polymorphism and exists in three forms designated α, β, and γ.[26,27] The low yielding β- and γ-polymorphs have attracted little attention since their first report in 1931. The α-polymorph, which is the most stable form at ambient pressure, crystallizes in the monoclinic space group $P2_1/c$. Similar to other zwitterionic dipeptides, the digly molecule crystallizes in a layered structure held together by hydrogen bonds (H-bonds). A single crystal neutron diffraction study by Kvick et

al. in 1977 obtained precise information about the coordinates of the hydrogen atoms in α-digly.[28] Later work probed the Raman spectra of this molecule near standard conditions.[29] Recently, Moggach et al. investigated the structure of α-digly under pressure and found the crystal structure to remain stable up to 4.7 GPa.[20] They noted that their crystal specimen began to "break up" above 5.4 GPa, which they attributed to a possible phase transition.

Further investigation of the proposed phase transition in digly and its high-pressure EOS is warranted for at least two reasons. First, the high-pressure EOS is necessary for thermochemical modeling of oligomerization reactions and phase transitions in high-pressure origin of life scenarios.[30] Second, molecules that exhibit multiple competing hydrogen-bonding (H-bonding) interactions such as digly are known to undergo a wide variety of transformations under pressure.[1] Identifying and understanding these changes in H-bonding is important as it controls the packing of amino acids and proteins, allowing multiple phases and conformations with different stabilities, solubilities, and physical properties.[31] Insights gained from quantifying these changes in relatively simple molecules such as digly could yield a more generalized physicochemical understanding that may be applicable to other systems.

High-pressure powder X-ray diffraction (PXRD) in a diamond anvil cell (DAC) has become a common technique for studying the behavior of materials under extreme pressure conditions. It is straightforward to extract reliable unit cell parameters and observe compressibility changes that may indicate structural phase transitions. Vibrational spectroscopy techniques, such as Raman, are also extremely useful for characterizing pressure-induced changes in materials. However, organic molecules often crystallize in low-symmetry forms, which makes it difficult to discern the exact nature of subtle conformational rearrangements or H-bonding changes at high pressures from these techniques. When high-pressure single-crystal or neutron diffraction experiments are impractical or their results inconclusive, computational chemistry offers a valuable route to predict crystal structures and help resolve experimental uncertainties. Crystal structure prediction codes such as USPEX combined with first-principles density functional theory (DFT) calculations are particularly useful for determining enthalpic drivers for phase transitions while simultaneously yielding lattice parameters and atomic positions.

Here we present a combined experimental and theoretical investigation of α-digly up to 14.5 GPa. Through synchrotron angle dispersive PXRD, we identify a change in the compressibility of the unit cell axes above ~6.7 GPa. While a discontinuity in the $P-V$ curve is not observed, above this pressure there is a clear change in slope relative to DFT predictions, which might indicate a change in compressibility. As there is no change in symmetry at the transition pressure, we hypothesize an isosymmetric phase transition occurs. A distinct change in the high-frequency Raman spectra between 6 and 7.5 GPa corroborates a change in bonding in this pressure range. To investigate the stability of other potential high-pressure polymorphs, we perform a structure search using the evolutionary structural search algorithm USPEX, which identifies a stable high-pressure monoclinic structure, α'-digly. The structure of α'-digly differs from that of α-digly only by a slight conformational change involving a rotation of the terminal amine group and a change in the H-bonding network.

Quantum-based EOS calculations on both structures show that α'-digly should exhibit a significantly longer c-axis compared to α-digly, which is in qualitative agreement with the experimentally observed axial change in compressibility. We hypothesize that α'-digly is indeed the phase we observe experimentally.

METHODS

Experiments. High-purity glycylglycine (Sigma-Aldrich, >99.9% purity) was used for all experiments in this study. The polymorphic purity of the as-received samples was confirmed by PXRD at ambient conditions. The as-received polycrystalline powder was ground to a fine powder in air using an agate mortar and pestle prior to high-pressure PXRD experiments. Rhenium gaskets, preindented to 40−45 μm thick by using 300 μm culets, were used to radially confine the samples. Initial sample chamber diameters were ~175 μm. The sample and pressure sensors (gold and ruby) were loaded into a DAC, which was high-pressure gas loaded with neon as a hydrostatic pressure transmitting medium (PTM).[32] For Raman experiments, argon was used as PTM. The sample chamber pressure was determined from the known ambient temperature EOS of gold[33] or ruby luminescence,[34] and the error in reported pressure is based on the variation of pressure within the cell.

X-ray diffraction experiments were performed at beamlines 13-ID-D and 13-BM-C, GeoSoilEnviroCARS at the Advanced Photon Source, Argonne National Laboratory. At 13-ID-D, we used an incident wavelength of 0.2952 Å and an X-ray diameter of ~2−4 μm, and powder diffraction images were obtained on a Pilatus 1M CdTe detector. Additional details on the XRD experimental setup are given in Prakapenka et al.[35] At 13-BM-C, we used an incident wavelength of 0.434 Å, an X-ray vertical × horizontal focus spot size of 20 μm × 15 μm, and collected powder diffraction images on a MAR165 charge coupled device (CCD) detector (Rayonix).[36] All experimental diffraction data were integrated by using DIOPTAS to yield scattering intensity vs 2θ patterns.[37] Analysis of the X-ray diffraction patterns via Rietveld refinement was performed by using GSAS II.[38] Positional parameters were fixed due to the high background from the DAC and preferred orientation effects of the crystallites. Crystal structure visualization was performed by using DIAMOND.[39] The weighted EOS was determined by using the program EosFit7c.[40]

Raman measurements were performed using the 514.5 nm line of an Ar ion laser for excitation in the backscattering geometry. The laser probe diameter was ~2 μm. Raman spectra were collected with a spectral resolution of 2 cm^{-1} using a single-stage grating spectrograph equipped with a liquid nitrogen cooled CCD array detector. Ultralow-frequency bandwidth solid-state notch filters allowed us to measure Raman spectra to within 10 cm^{-1} of the Rayleigh line.

Computations. Digly was investigated by using density functional theory (DFT)[41,42] as implemented in the Vienna Ab initio Simulation Package[43] (VASP) using projector-augmented wave (PAW) pseudopotentials.[44,45] The Perdew−Burke−Ernzerhof (PBE)[46] generalized gradient approximation functional was used[44,45] with the Grimme D2 empirical correction (PBED2) to account for van der Waals forces that are poorly described by DFT.[47−49] PBE with van der Waals empirical correction has previously been shown to yield fairly good results compared to experiment for the EOS and vibrational properties of other CHNO molecular crystals.[50,51]
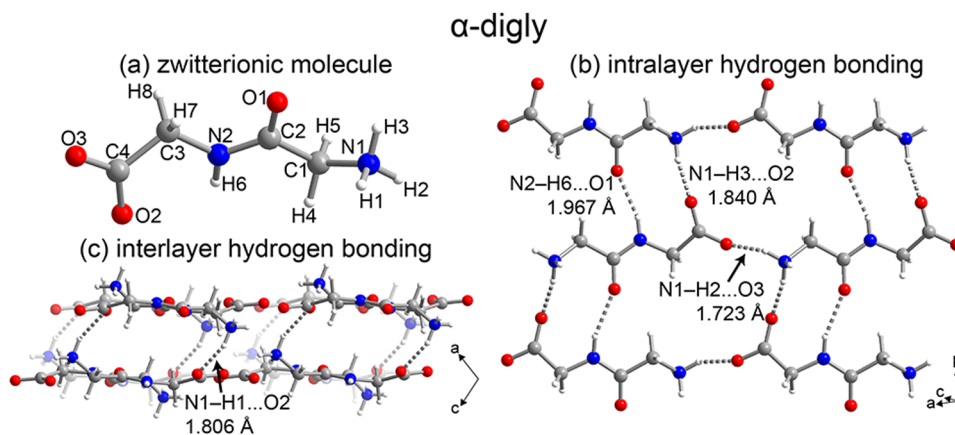
Figure 1. (a) The digly zwitterionic molecule with atom labels. (b) The structure of α-digly viewed from the $a-b$ projection highlighting the intralayer H-bonds. (c) The $a-c$ projection highlighting the interlayer H-bond interactions. H-bond distances are taken from the crystal structure determined in a previous study by low-temperature (82 K) neutron diffraction.[28]

Because of the inadequate description of electron correlation and other effects, the PBE functional also typically overestimates the length of covalent bonds and underestimates the length of hydrogen bonds.[52−54] An assessment on the accuracy of the PBE functional on H-bonded systems such as water has been performed elsewhere.[53−58]

Optimized lattice parameters, atomic configurations, and hydrostatic pressure were obtained as a function of volumetric compression ratio V/V_0 at $T = 0$ K. The equilibrium volume V_0 was calculated at ambient pressure, and the volume was reduced sequentially in increments of $0.02V_0$. The wave function was calculated with an 800 eV plane-wave energy cutoff and k-point density of 0.05 Å^{-1} for the smallest volume studied. The self-consistent field accuracy threshold was set to 1×10^{-7} eV, and optimizations of the ionic degrees of freedom were performed with a force-based accuracy threshold of 7×10^{-3} eV/Å. The zero-point energy (ZPE) contribution to the energy and pressure was also calculated. The ZPE was calculated at each volume increment through the quasi-harmonic approximation from the vibrational normal modes obtained at the Γ-point using the finite displacement method implemented in VASP VTST tools. Finite displacement calculations were performed using the unit cell, which is quite large (lattice parameters 7−10 Å). However, it is possible that errors in the force associated with periodic images of displacements are present. For this reason, we do not add the thermal contribution to the energy or pressure using the quasi-harmonic approximation because it will likely require a larger supercell which is too computationally expensive. Adding the ZPE is intended to give better agreement with experiment while still being a tractable calculation. The pressure associated with the ZPE was added to the cold pressure to obtain the EOS. The ZPE pressure was calculated by taking the derivative of the ZPE with respect to the volume.

A molecular crystal structure search for possible polymorphs of digly was performed at 10 GPa by using the first-principles evolutionary crystal structure prediction method USPEX.[59−61] The enthalpies were calculated with a similar DFT approach for the USPEX search as for the EOS calculation described above, with exceptions noted below. The lattice parameters are also measured in the XRD patterns which gives a good estimate for the number of formula units. Therefore, the search was performed with 4 formula units (or digly molecules) in the

unit cell. This implies that only unit cells or primitive cells with 4 formula units, or supercells with 1 or 2 formula units, are explored in the search. While this implies that not every configuration is explored (with a different number of formula units), 4 formula units covers a large portion of the energy landscape and is the same number of formula units contained in the α-digly unit cell. Using more formula units in the search is prohibitive in terms of computational cost. Furthermore, in the subset of structures that are explored we can identify whether there exists energetically competitive structures at high pressures. The search was performed with a population size of 50 for seven generations. A plane-wave energy cutoff of 450 eV and k-point density of 0.08 Å^{-1} were used during the search for increased computational efficiency.

■ **RESULTS AND DISCUSSION**

Effect of Pressure on α-Digly from PXRD and Raman. At ambient conditions, α-digly crystallizes in a layered structure in the $P2_1/c$ space group (SG number 14, $Z = 4$, Figure 1). The ambient experimental and calculated lattice parameters show excellent agreement (Table 1). Each digly molecule in the α-phase exhibits four H-bonding interactions. One H-bond from the peptidic nitrogen (N2−H6···O1) and two H-bonds from the terminal nitrogen (N1−H2···O3 and N1−H3···O2) are formed between molecules in the same layer (Figure 1b). These layers stack approximately along the c-axis

Table 1. Measured and Calculated Lattice Parameters of α-Digly[20] [a]

parameter	expt (ambient, this study)	expt (SC data)[20]	theory	diff (%)
a (Å)	8.141(2)	8.123(2)	8.0648	−0.9
b (Å)	9.5882(8)	9.554(2)	9.5209	−0.7
c (Å)	7.844(2)	7.822(2)	7.7980	−0.6
β (deg)	107.670(5)	107.596(4)	106.2248	−1.3
V (Å^3)	583.41(5)	578.7(2)	574.92	−1.5

[a]Errors are shown in parentheses. Lattice parameters from a previous single crystal study are given for comparison. Calculated lattice parameters are at 0 GPa and 0 K with ZPE contributions added. The percent difference is between experimental and theoretical ambient parameters from this study.
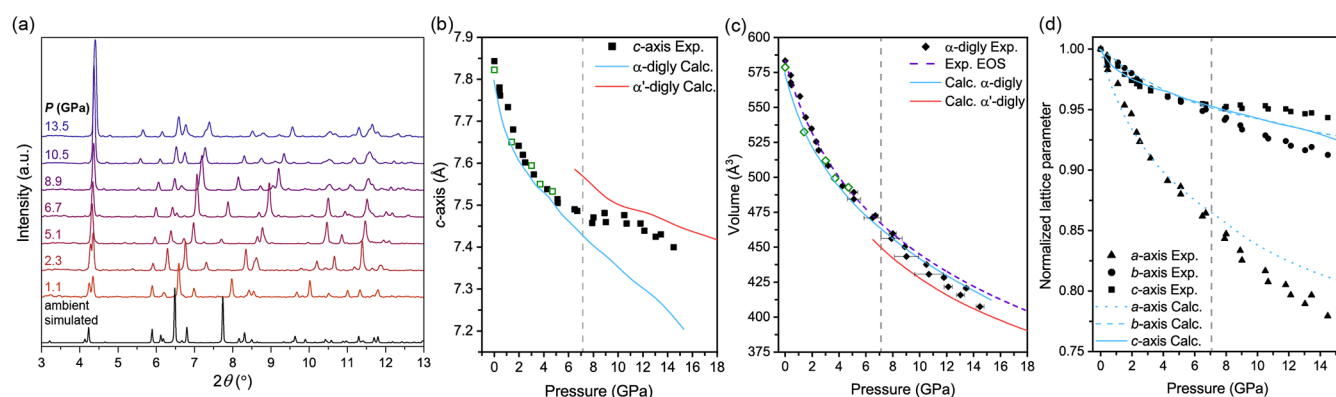
Figure 2. (a) Selected PXRD patterns of digly as pressure is increased ($\lambda = 0.434$ Å) and an ambient pressure simulated pattern for comparison. Patterns have been background subtracted and scaled in intensity for clarity. Values of the c-axis (b) and unit cell volume (c) of digly upon quasi-hydrostatic compression and the normalized unit cell axes (d) as a function of pressure. Experimental data from this study are denoted by black filled symbols, while data from a previous study by Moggach et al. are denoted by green open symbols.[20] Calculated values are shown for α-digly and α'-digly in blue and red solid lines, respectively. The gray dashed line indicates where the compressibility change is observed. The experimentally determined EOS for the entire data range is shown by a violet dashed line in (c).

and are connected by the fourth H-bond from the terminal nitrogen atom (N1−H1···O2, Figure 1c).

To probe the structural changes of α-digly upon quasi-hydrostatic compression, we performed high-pressure X-ray diffraction (XRD) experiments to a maximum pressure of 14.5 GPa using a DAC. Figure 2 shows the evolution of the PXRD patterns at selected pressures. We do not observe the appearance or disappearance of Bragg peaks upon compression, and the patterns are well modeled in the monoclinic $P2_1/c$ space group at all pressures. The changes in relative intensity of peaks during compression can be attributed to preferred orientation effects (e.g., sampling crystallites at different orientations) and the merging or separation of peaks.

To investigate the possibility of a pressure-induced phase transition, the diffraction patterns were analyzed by performing Rietveld refinements using the GSAS-II software (Figure S2).[38] Because of the relatively large number of atoms and the low scattering power of the sample, full structure refinements were not feasible and only the lattice parameters and unit cell volume were determined at each pressure (Figure 2). The low-pressure (ambient to 6.7 GPa) compression behavior of the unit cell axes is in agreement with previous experimental structural studies,[20] with the a-axis being the most compressible and the b- and c-axes having nearly identical compressibilities. The a- and b-axes vary monotonically with pressure, whereas there is a distinct discontinuity in the pressure dependence of the c-axis between 8 and 9 GPa (Figure 2b). This axial compressibility change does not lead to a significant discontinuity in the overall P−V curve. However, it is not clear from the experimental data alone whether there is an associated change in the slope of the volume with pressure (Figure 2c).

The observed behavior could be rationalized by a concomitant relaxation along the a- and b-axes, which would compensate for the stiffening along the c-axis. To test this hypothesis, we calculated the expected lattice parameters and volume as a function of pressure for α-digly using DFT and compared it to the normalized experimental data (Figure 2c and Figure S3b). From ambient pressure to ∼6.7 GPa, the experimental and predicted lattice parameters and volume match extremely well. Above this pressure, the experimental data show a significant break in slope from what is predicted by

DFT. The c-axis becomes noticeably less compressible than what is expected from calculations, while the a- and b-axes become more compressible. Comparison of the normalized volumes shows that above ∼8 GPa the experimental data fall below the DFT predictions (Figure S3b).

The observation that α-digly undergoes a change in axial compressibility above 6.7 GPa invalidates the fitting of a single EOS to the P−V data.[62,63] Therefore, we determined the experimental EOS model parameters for α-digly from ambient pressure to 6.7 GPa using a weighted third-order Birch−Murnaghan (B−M) EOS least-squares fit of the P−V data using EoSFit7 (Table 2).[40] We fixed V_0 to the value

Table 2. Comparison of Experimental and Theoretical Third-Order Birch−Murnaghan (BM) EOS Parameters for α-Digly[a]

calc/expt	press. range (GPa)	V_0 (Å³)	B_0 (GPa)	B_0'
expt	0−6.7	583.41(5)	16(1)	6.1(9)
calc	0−6.5	573.27	14.6	8.2
calc	0−15.3	572.38	16.9	6.4

[a]The BM fits using the theoretical results were performed in two different pressure ranges: one to match the pressure range from experiment and another by using the full curve.

determined from Rietveld refinement of the ambient PXRD pattern (583.41(5) Å³), which agrees well with the value previously determined from single-crystal X-ray diffraction experiments (578.7(2) Å³).[20] The fitted bulk modulus (B_0) and the pressure derivative (B_0') for the low pressure range of experimental and calculated data agree well (Table 2).

Raman spectroscopy is a widely used tool for in situ high-pressure characterization of organic material due to its high spatial resolution and sensitivity to both structural and chemical changes. Raman spectra of α-digly were measured at several pressures to obtain additional characteristics not revealed by PXRD that might explain the change in compressibility. Figure 3 shows the Raman spectra of α-digly at different pressures and the frequency of modes as a function of pressure for the high wavenumber region (2850−3350 cm⁻¹). There are six modes in this region at ambient pressure, which are stretching vibrations of C−H and N−H. Because of
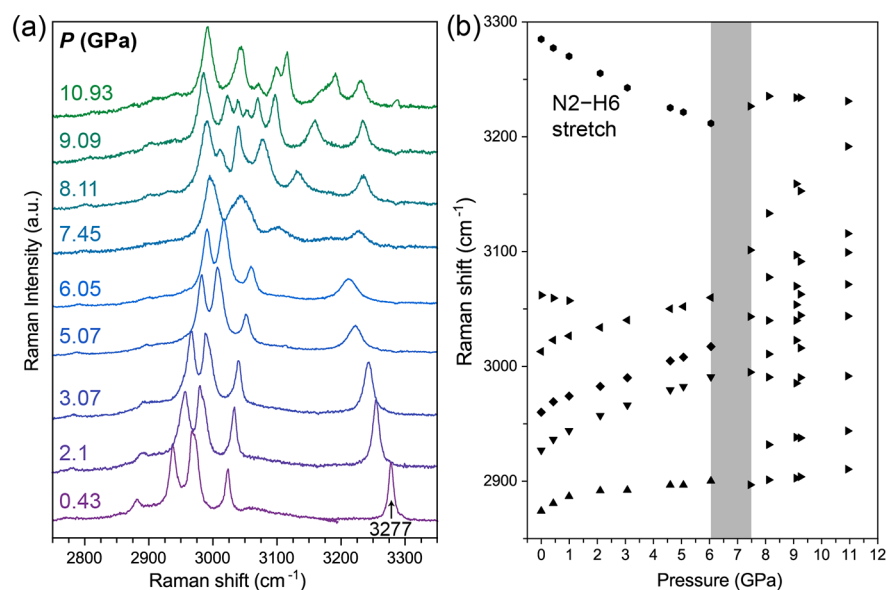
Figure 3. Raman spectra of α-digly shown at selected pressures (a) and the Raman modes frequencies as a function of pressure (b) for the high-frequency wavenumber region from 2850 to 3350 cm^{-1}. The proposed transition pressure (6−7.5 GPa) is noted by a gray box in (b). Above the transition pressure, modes disappear, new modes appear, and many existing modes abruptly change slope.

discrepancies with mode assignments in previous publications,[29,64] only the widely accepted peptide N2−H6 stretching mode is labeled in the figure at 3277 cm^{-1}. Most of the modes exhibit typical blue-shifting from ambient pressure to ∼6 GPa; however, the N2−H6 stretching mode red-shifts as pressure is increased at a rate of 12.1(3) cm^{-1}/GPa (Figure S4). This is associated with an increase in the strength of the N2−H6···O1 H-bonding interaction as pressure is increased, which we hypothesize occurs because there is no other competing H-bonding interaction with O1. Beginning at 7.45 GPa, we observe a change in the high-frequency Raman spectra, which includes splitting of modes and a change in the pressure-dependent shift of some modes. At this pressure we also observe the appearance, disappearance, and change in pressure−frequency slope of modes in other regions of the spectra (Figures S5 and S6). Notably, there is little change in the number of lattice modes, which combined with the diffraction data indicates that the new phase has the same structural complexity; i.e., the modification does not result in a change of symmetry (Figure S5). The pressure range in which distinct changes are observed in both PXRD and Raman is similar, supporting the conclusion that a conformational change occurs between 6 and 9 GPa.

The aggregate of experimental PXRD and Raman data clearly indicates a change in the response of the α-digly structure to pressure arises above 6 GPa. In addition, both experiments support that the $P2_1/c$ symmetry is maintained through the transition. The changes in slope of the lattice parameters and volume, along with the changes in the slope of several Raman modes with pressure, suggest a phase transition. Because the change in the compression mechanism is not accompanied by a symmetry change, it is considered to be an isosymmetric phase transition.[62,65,66] This has been observed in a number of other systems, including a pressure-induced isosymmetric conformational change in the amino acid L-serine.[21] The data support the hypothesis that a conformational phase transition occurs at this pressure that only affects

the packing, compressibility, short-range order, and H-bonding of the molecule.

Insights from USPEX and DFT Calculations. To gain further insight into the behavior of the lattice parameters upon compression and complement our understanding of the experimental data, we performed a first-principles structural search of polymorphs of digly at 10 GPa with USPEX using 4 formula units. Several structures were found that are lower in enthalpy than α-digly. The structure lowest in enthalpy is in space group $P2_12_12_1$ (digly-$P2_12_12_1$), while another structure is nearly identical to α-digly in space group $P2_1/c$ (α′-digly) (Figure 4). Both have 4 formula units of diglycine in the unit cell. The orthorhombic $P2_12_12_1$ crystal consists of digly molecules that are significantly bent approximately around the peptide bond and pack in a much denser arrangement (Figure S7). The energetic cost to bend the digly molecules is apparently more than offset by a reduction in the enthalpy
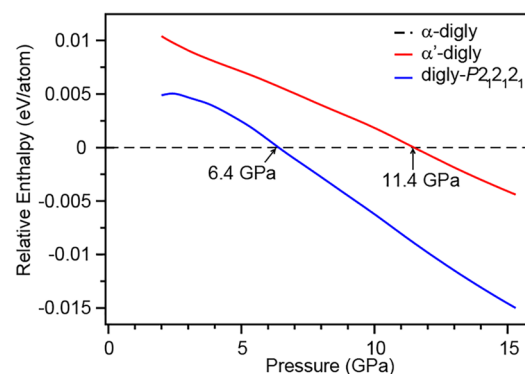

Figure 4. Relative enthalpy including ZPE at 0 K as a function of pressure for α-digly compared to α′-digly up to 15 GPa. α-digly is predicted to transform into α′-digly above a pressure of 11.4 GPa. Another orthorhombic phase (digly-$P2_12_12_1$) is predicted to be lower in enthalpy than α-digly and α′-digly above 6.4 GPa, but was not observed in experiment.
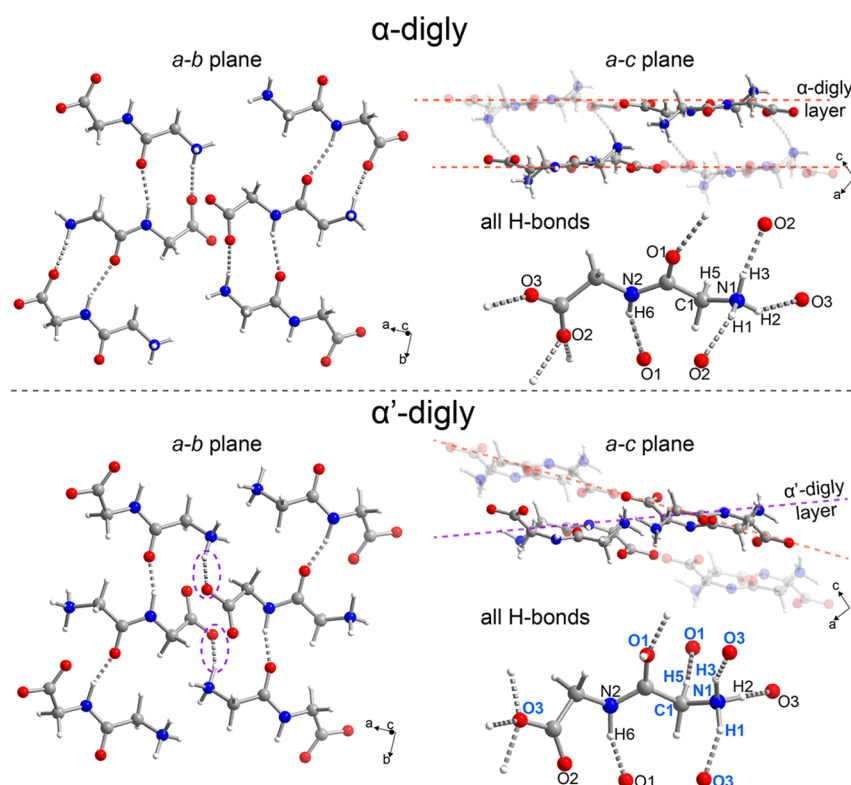
Figure 5. Comparison of the molecular packing and H-bond interactions in the ambient experimental α-digly crystal structure (top) and the calculated 13.75 GPa α′-digly crystal structure (bottom). Atoms in α′-digly that exhibit a change in H-bonding compared to α-digly are labeled in bold blue font in the bottom panel. The most notable difference between the two structures is the change in interlayer bonding and the existence of a C1−H5···O1 interaction in α′-digly. H-bonding interactions forming the new layers are denoted by a violet circle.

through a smaller volume and hence the PV term. Digly-$P2_12_12_1$ is predicted to become lower in enthalpy than α-digly above 6.4 GPa. The simulated PXRD pattern of digly-$P2_12_12_1$ is significantly different from that of α-digly (Figure S8). We do not observe experimentally the appearance of new peaks that would be expected from the formation of digly-$P2_12_12_1$. Thus, we conclude that this orthorhombic structure is not formed under the conditions investigated in this work, likely due to a large energy barrier for the transition associated with the significant change in packing, concerted bending the peptide backbone, and disruption to the H-bonding network.

A second structure was also found in our USPEX search, which we refer to as α′-digly. This structure has the same monoclinic $P2_1/c$ symmetry as α-digly and can be thought of as a slight conformational distortion from the original crystal packing (Figure 5). In the structure search, α′-digly is originally lower in enthalpy at 10 GPa when ZPE is not included in the enthalpy. However, after the structure search was completed, the ZPE was added which increases the enthalpy of α′-digly compared to α-digly, which increases the pressure where the enthalpies are equal to 11.4 GPa (Figure 4). In fact, above 15 GPa, DFT-level conjugate-gradient optimizations of α-digly yield α′-digly, which indicates that α-digly is no longer a stable minimum on the potential energy surface and that the barrier for the transition is negligible above about 15 GPa. This also qualitatively indicates the energy barrier associated with the α to α′ transition is not too large for it to occur in room-temperature experiments at pressures lower than 15 GPa. This is because the bending of the peptide backbone as well as the change in the overall packing of the structure is less significant for α′ than it is for digly-$P2_12_12_1$.

We calculated the lattice parameters and volume as a function of pressure for α′-digly to gauge how they compare to the calculated values for α-digly and those determined from experiment (Figure 2b,c and and Figure S3a). At 10 GPa, the calculated α-digly a-axis is 0.43 Å longer than that of α′-digly, while the c-axis is 0.15 Å shorter than that calculated for α′-digly. The differences in the calculated a- and c-axes between the polymorphs agree with the experimentally observed changes in compressibility. On the other hand, the calculated α′-digly b-axis is 0.08 Å longer than that of α-digly, which disagrees with the experimental observation of a more compressible b-axis. One source for this discrepancy could be that the b-direction entirely consists of H-bonded sheets of digly molecules and as such contain multiple H-bonding interactions, which DFT struggles to model very accurately. Additionally, a difference in thermal expansion of both phases could account for this small discrepancy. While we cannot irrefutably conclude that the calculated structure of α′-digly is observed experimentally, we hypothesize that this is the phase observed in experiment. Although the transition pressure of 11.4 GPa is higher than the observed transition of 6.7 GPa, the enthalpy of α′-digly is very close to the enthalpy of α-digly in the 6−9 GPa range (<10 meV/atom). Because the PBE functional (with D2 correction) gives a somewhat poor description of H-bonding, it is expected that DFT is unable to predict the relative enthalpy exactly. Generally speaking, predicting the relative free energies of molecular crystal polymorphs is very challenging. This can be seen in a recent review article on the subject where the PBE level of theory incorrectly predicts β phase of glycine to be the lowest energy polymorph.[67] Incorrect rankings are found for other

polymorphs as well. Additional challenges are described in detail in the fifth and sixth blind tests for organic crystal structure prediction.[68,69] In addition, since the crystal packing of both structures is very similar, it is possible that thermal fluctuations could promote the local existence of the α'-phase below the calculated phase transition pressure. Overall, calculations support the hypothesis that a change in H-bonding and a conformational change could lead to an isosymmetric phase transition.

The major differences between the crystal structure of α-digly and the predicted crystal structure of α'-digly arise from a change in the H-bonding interactions concomitant with a slight rotation of the functional groups and a change in molecular packing. To highlight the difference between the two structures, we compare the ambient experimental crystal structure to the predicted 13.75 GPa structure of α'-digly (Figure 5). For clarity, relevant atoms involved in the hydrogen-bonding interactions have been numbered and labeled (Figures 1 and 6, Figure S1). As described in detail
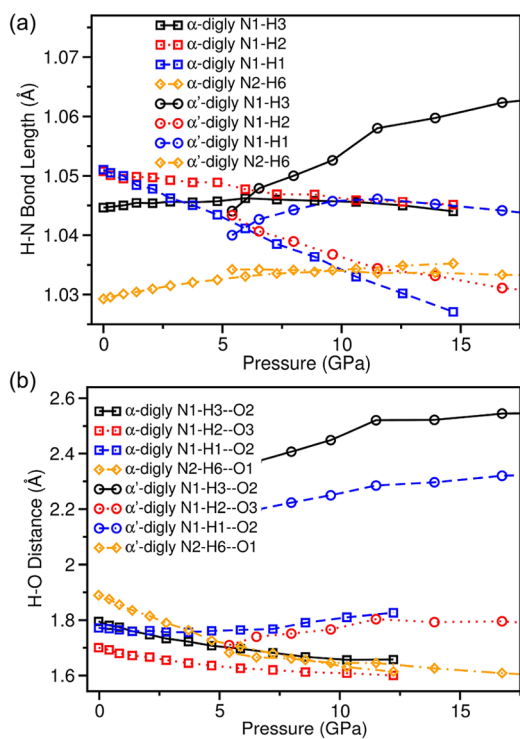

Figure 6. Calculated bond lengths between (a) hydrogen and nitrogen in the amine group and (b) the N−H⋯O H-bond length in α-digly and α'-digly as a function of pressure. To show how the bond changes for both conformers, the color of the line is the same for both conformers for the same bond. Additional H-bonds in α'-digly are not shown for clarity. A weakening of the H-bonding causes the N1−H1 bond length to decrease significantly from 0 to 10 GPa and the increases the N1−H1⋯O2 bond slightly from 0 to 10 GPa.

above, each α-digly molecule exhibits three intralayer H-bonding interactions and one interlayer H-bonding interaction. The primary H⋯O distances in each structure are summarized in Table S1. In the predicted α'-digly crystal structure, there is a change in H-bonding interactions that results in a rotation of the terminal amine group at the molecular level and a change in the layering of the molecules (Figure 5). In the new structure, there are only two intralayer H-bonds. The shortest

H-bonding interaction is calculated to be between the peptidic nitrogen and the oxygen atom of the molecule within that layer (N2−H6⋯O1, 1.63 Å). The second, longer intralayer H-bond is from the terminal amine to a carboxylic oxygen atom of another molecule (N1−H3⋯O3, 1.66 Å). These shortest interactions make up the new layers in the structure (Figure 5, side view). In α'-digly, there are three interlayer H-bonds. Two are between the terminal amine hydrogens and the carboxylic oxygen atom (N1−H1⋯O3, 1.74 Å, and N1−H2⋯O3, 1.78 Å). Notably, there is a third, new interaction, C1−H5⋯O1 (1.74 Å), which competes with the H-bonding interaction of the peptidic nitrogen (N2−H6⋯O1). Overall, α'-digly represents a modest conformational and layering change from α-digly.

In previous studies, it has been noted that extremely short H-bonds will not form through the application of moderate (1−10 GPa) pressures.[20,21] Instead, if a H-bond length approaches some lower limit, which is specific for each kind of interaction (e.g., N−H⋯O and C−H⋯O), the molecule will undergo a conformational phase transition such that it avoids forming extremely short H-bonds. This behavior was observed for the isosymmetric phase transition in L-serine, which occurs once the N⋯O separation in the N−H⋯O H-bond reaches the critical distance of 2.691(13) Å at 4.8 GPa.[21] In the case of α-digly, Moggach et al. comment that the N1−H2⋯O3 interaction is extremely short at 4.7 GPa.[20] We hypothesize that like in the case of L-serine, a phase transition occurs in α-digly above ∼6.7 GPa, which reorients the molecule so that it avoids a very short N1−H2⋯O3 H-bonding interaction. At some critical point, one can imagine this compression mechanism becoming energetically unfavorable and the rotation of the amine groups being initiated. In this way, the conformation change may occur to relax a strained H-bonding interaction.

To support this argument, we computed the relevant H-bond lengths, N1−Hn and N1−Hn⋯O, in α- and α'-digly as a function of pressure (see Figure 6). Several notable changes occur as a function of pressure. In α-digly, the N1−H1 bond length decreases substantially as a function of pressure while N1−H2 and N1−H3 bond lengths do not change much with pressure (Figure 6a). However, in α'-digly N1−H1 is larger and increases with pressure. The H⋯O bond lengths tend to decrease as a function of pressure in α-digly, indicating a strengthening of the hydrogen bonding, except for N1−H1⋯O2, which increases slightly with pressure (Figure 6b). Because the N1−H1⋯O2 length does not decrease with pressure, this causes the corresponding N1−H1 bond length to sharply decrease with pressure. Because of the rotation of the amine group in α'-digly, the hydrogen bonding in the two structures is quite different. The N1−H2⋯O3 and N1−H1⋯O2 hydrogen bond lengths increase by over 0.2 Å in α'-digly. These calculated changes support the hypothesis that a phase transition occurs to relax strained H-bonding interactions.

Analysis of charges was performed using the Mullikan and DDAP methods to gauge chemical differences between α- and α'-digly.[70,71] This reveals a charge transfer in the carbon−nitrogen backbone structure (Table S3). Perhaps the most notable feature is the electron transfer from carbon atom C4 (on the carboxylic group) to C3, which simultaneously strengthens the C3−C4 bond and weakens the C3−N2 bond. This charge transfer helps enable the bending of the peptide backbone of the digly molecule in α'-digly. To better understand the changes in the α-digly molecule under

pressure, maximally localized Wannier functions and the eigenvalue of each wave function center were calculated (Figure S9).[72] Each eigenvalue increases at higher pressures, which is expected. The lowest eigenvalue and strongest bond is the C3−N2 bond, while the highest eigenvalue is the H···O hydrogen bonds (Figure S9). This indicates possible reactivity of the O atom. The difference in atomic charges in α'-digly demonstrates it is chemically different than α-digly.

The predicted pressure-dependent Raman spectra (Figures S10 and S11) and bond lengths (Figure 6) of α-digly are qualitatively consistent with the experimental Raman spectra. Mode assignments are made at ambient pressure (Table S2), but the modes are difficult to track as a function of pressure because there is significant mode crossing in the high-frequency range. The calculated Raman spectra also show the red-shift of the peptidic N2−H6 stretching mode and a significant blue-shift of the N1−H1 NH_3 stretching mode (Figure S11). The blue-shift of the N1−H1 NH_3 stretching mode is due to the decrease in the N1−H1 bond length (Figure 6a), and the red-shift of N2−H6 is due to the increase in the N2−H6 bond length (Figure 6b). The calculated Raman spectra show these modes crossing one another (Figure S11). The red-shift of the peptidic N2−H6 mode is consistent with experiment (Figure 3b); however, it is not clear whether the crossing of the peptidic N2−H6 mode with N1−H1 NH_3 mode occurs in experiment (Figure 3a). For α'-digly, the calculated Raman spectra show some red-shifted modes compared to α-digly at 10 GPa (Figure S11). This is due to the larger bond length in N1−H2 in α'-digly compared to N1−H1 for α-digly and the larger bond length N1−H3 in α'-digly. The substantial changes in the Raman spectra and bond lengths demonstrate the impact strengthening/weakening H-bonding can have on the structure and vibrational properties of these types of H-bonded materials.

CONCLUSIONS

The high-pressure response of the simplest dipeptide α-glycylglycine (α-digly) was investigated up to 14.5 GPa through a combined experimental and computational chemistry effort. A change in the compressibility of the lattice parameters was identified upon quasi-hydrostatic compression above ∼6.7 GPa via high-pressure powder X-ray diffraction (PXRD) experiments using a diamond anvil cell. No associated abrupt change in symmetry was observed, suggesting an isosymmetric phase transition. We determine the equation of state parameters for the low-pressure range, which matches extremely well with density functional theory (DFT) predictions. Changes in the slope and number of Raman modes as a function of pressure between 6 and 7.5 GPa corroborate that a phase transition occurs in this pressure range. The observation that these changes occur around the same pressure in the PXRD and Raman experiments further supports the assignment of an isosymmetric phase transition between 6 and 7.5 GPa. We performed a detailed structure search using the evolutionary structural search algorithm, USPEX to identify stable high-pressure phases and aid interpretation of the experimental data. We found an orthorhombic structure that is calculated to be the lowest enthalpy polymorph above 6.8 GPa. However, this structure is inconsistent with experimental data, as the XRD patterns are indexed with a monoclinic structure for the full pressure range. We also identified an isosymmetric monoclinic modification of α-digly, α'-digly, which should exhibit a significantly longer c-

axis compared to α-digly and is predicted to be lower in enthalpy than α-digly above 11.4 GPa. Based on the similarity of the compressibility changes observed experimentally, this is the best candidate phase. The DFT predictions suggest the isosymmetric phase transition involves a change in the H-bonding network as well as a bent peptide backbone in the digly molecule. Calculations show that the digly molecule is chemically different in α'-digly compared to α-digly due to the bent peptide backbone and a charge transfer that takes place within the molecule. The unique chemical structure of α'-digly thus makes it relevant for investigating the formation of polypeptides at high pressures. Future experiments, such as single-crystal X-ray diffraction and neutron diffraction studies, will be useful in experimentally confirming the exact conformational changes that occur in α-digly under pressure.

■ ASSOCIATED CONTENT

ⓈSupporting Information

The Supporting Information is available free of charge at https://pubs.acs.org/doi/10.1021/acs.jpcb.9b07313.

Figures S1−S11 and Tables S1−S3 (PDF)

X-ray crystallographic data of α'-digly (CIF)

X-ray crystallographic data of digly-$P2_12_12_1$ (CIF)

■ AUTHOR INFORMATION

Corresponding Authors
*E-mail clarke30@llnl.gov. Tel 925-422-6969.
*E-mail steele26@llnl.gov. Tel 925-422-9902.

ORCID ⓘ
Samantha M. Clarke: 0000-0002-6874-9929
Matthew P. Kroonblawd: 0000-0002-5009-5998
Dongzhou Zhang: 0000-0002-6679-892X
Elissaios Stavrou: 0000-0001-5212-4927

Notes
The authors declare no competing financial interest.

■ REFERENCES

(1) Fabbiani, F. P.; Pulham, C. R. High-pressure Studies of Pharmaceutical Compounds and Energetic Materials. *Chem. Soc. Rev.* **2006**, *35*, 932−942.

(2) Hazen, R. M.; Boctor, N.; Brandes, J. A.; Cody, G. D.; Hemley, R. J.; Sharma, A.; Yoder, H. S. High Pressure and the Origin of Life. *J. Phys.: Condens. Matter* **2002**, *14*, 11489−11494.

(3) Daniel, I.; Oger, P.; Winter, R. Origins of Life and Biochemistry under High-pressure Conditions. *Chem. Soc. Rev.* **2006**, *35*, 858−875.

(4) Ohara, S.; Kakegawa, T.; Nakazawa, H. Pressure Effects on the Abiotic Polymerization of Glycine. *Origins Life Evol. Biospheres* **2007**, *37*, 215−223.

(5) Lemke, K. H.; Rosenbauer, R. J.; Bird, D. K. Peptide synthesis in early Earth hydrothermal systems. *Astrobiology* **2009**, *9*, 141−146.

(6) Pedreira-Segade, U.; Hao, J.; Montagnac, G.; Cardon, H.; Daniel, I. Spontaneous polymerization of glycine under hydrothermal conditions. *ACS Earth and Space Chemistry* **2019**, *3*, 1669−1677.

(7) Goldman, N.; Reed, E. J.; Fried, L. E.; William Kuo, I.-F.; Maiti, A. Synthesis of Glycine-containing Complexes in Impacts of Comets on Early Earth. *Nat. Chem.* **2010**, *2*, 949.

(8) Chyba, C.; Sagan, C. Endogenous Production, Exogenous Delivery and Impact-shock Synthesis of Organic Molecules: An Inventory for the Origins of Life. *Nature* **1992**, *355*, 125−132.

(9) Sugahara, H.; Mimura, K. Glycine Oligomerization up to Triglycine by Shock Experiments Simulating Comet Impacts. *Geochem. J.* **2014**, *48*, 51−62.

(10) Sugahara, H.; Mimura, K. Peptide Synthesis Triggered by Comet Impacts: A Possible Method for Peptide Delivery to the Early Earth and Icy Satellites. *Icarus* **2015**, *257*, 103−112.

(11) Otake, T.; Taniguchi, T.; Furukawa, Y.; Kawamura, F.; Nakazawa, H.; Kakegawa, T. Stability of Amino Acids and Their Oligomerization under High-pressure Conditions: Implications for Prebiotic Chemistry. *Astrobiology* **2011**, *11*, 799−813.

(12) Kroonblawd, M.; Lindsey, R.; Goldman, N. Synthesis of Functionalized Nitrogen-containing Polycyclic Aromatic Hydrocarbons and Other Prebiotic Compounds in Impacting Glycine Solutions. *Chem. Sci.* **2019**, *10*, 6091−6098.

(13) Moggach, S.; Parsons, S.; Allan, D. High-pressure Crystallographic Study of L-cysteine, the Route to a New Polymorph. *Acta Crystallogr., Sect. A: Found. Crystallogr.* **2004**, *60*, No. s251.

(14) Moggach, S. A.; Allan, D. R.; Clark, S. J.; Gutmann, M. J.; Parsons, S.; Pulham, C. R.; Sawyer, L. High-pressure Polymorphism in L-cysteine: The Crystal Structures of L-cysteine-iii and L-cysteine-iv. *Acta Crystallogr., Sect. B: Struct. Sci.* **2006**, *62*, 296−309.

(15) Moggach, S. A.; Parsons, S.; Wood, P. A. High-pressure Polymorphism in Amino Acids. *Crystallogr. Rev.* **2008**, *14*, 143−184.

(16) Hinton, J. K.; Clarke, S. M.; Steele, B. A.; Kuo, I.-F. W.; Greenberg, E.; Prakapenka, V. B.; Kunz, M.; Kroonblawd, M. P.; Stavrou, E. Effects of Pressure on the Structure and Lattice Dynamics of *α*-glycine: A Combined Experimental and Theoretical Study. *CrystEngComm* **2019**, *21*, 4457.

(17) Boldyreva, E. V.; Ivashevskaya, S. N.; Sowa, H.; Ahsbahs, H.; Weber, H.-P. Effect of High Pressure on Crystalline Glycine: A New High-pressure Polymorph. *Dokl. Phys. Chem.* **2004**, *396*, 111−114.

(18) Tumanov, N. A.; Boldyreva, E. V. X-Ray Diffraction and Raman Study of Dl-Alanine at High Pressure: Revision of Phase Transitions. *Acta Crystallogr., Sect. B: Struct. Sci.* **2012**, *68*, 412−423.

(19) Boldyreva, E. V.; Ivashevskaya, S. N.; Sowa, H.; Ahsbahs, H.; Weber, H.-P. Effect of Hydrostatic Pressure on the *γ* - Polymorph of Glycine 1. A Polymorphic Transition into a New *δ* -form. *Z. Kristallogr. - Cryst. Mater.* **2005**, *220*, 50−57.

(20) Moggach, S. A.; Allan, D. R.; Parsons, S.; Sawyer, L. Effect of Pressure on the Crystal Structure of *α*-glycylglycine to 4.7 GPa; Application of Hirshfeld Surfaces to Analyse Contacts on Increasing Pressure. *Acta Crystallogr., Sect. B: Struct. Sci.* **2006**, *62*, 310−320.

(21) Moggach, S. A.; Allan, D. R.; Morrison, C. A.; Parsons, S.; Sawyer, L. Effect of Pressure on the Crystal Structure of L-serine-i and the Crystal Structure of L-serine-ii at 5.4 GPa. *Acta Crystallogr., Sect. B: Struct. Sci.* **2005**, *61*, 58−68.

(22) Murli, C.; Sharma, S. M.; Karmakar, S.; Sikka, S. *α*-glycine under High Pressures: A Raman Scattering Study. *Phys. B* **2003**, *339*, 23−30.

(23) Dawson, A.; Allan, D. R.; Belmonte, S. A.; Clark, S. J.; David, W. I. F.; McGregor, P. A.; Parsons, S.; Pulham, C. R.; Sawyer, L. Effect of High Pressure on the Crystal Structures of Polymorphs of Glycine. *Cryst. Growth Des.* **2005**, *5*, 1415−1427.

(24) Kroonblawd, M. P.; Pietrucci, F.; Saitta, A. M.; Goldman, N. Generating Converged Accurate Free Energy Surfaces for Chemical Reactions with a Force-matched Semiempirical Model. *J. Chem. Theory Comput.* **2018**, *14*, 2207−2218.

(25) Kitadai, N. Thermodynamic Prediction of Glycine Polymerization As a Function of Temperature and Ph Consistent with Experimentally Obtained Results. *J. Mol. Evol.* **2014**, *78*, 171−187.

(26) Bernal, J. D. The Crystal Structure of the Natural Amino Acids and Related Compounds. *Z. Kristallogr. - Cryst. Mater.* **1931**, *78*, 363−369.

(27) Hughes, E. W.; Moore, W. J. The Crystal Structure of *β*-glycylglycine. *J. Am. Chem. Soc.* **1949**, *71*, 2618−2623.

(28) Kvick, Å.; Al-Karaghouli, A.; Koetzle, T. Deformation Electron Density of *α*-glycylglycine at 82 K. I. The neutron diffraction study*. *Acta Crystallogr., Sect. B: Struct. Crystallogr. Cryst. Chem.* **1977**, *33*, 3796−3801.

(29) Lagant, P.; Vergoten, G.; Loucheux-Lefebvre, M.; Fleury, G. Raman Spectra and Normal Vibrations of Dipeptides. I. Glycylglycine. *Biopolymers* **1983**, *22*, 1267−1283.

(30) Shock, E. L. Stability of Peptides in High-temperature Aqueous Solutions. *Geochim. Cosmochim. Acta* **1992**, *56*, 3481−3491.

(31) Steiner, T. The Hydrogen Bond in the Solid State. *Angew. Chem., Int. Ed.* **2002**, *41*, 48−76.

(32) Klotz, S.; Chervin, J.; Munsch, P.; Le Marchand, G. Hydrostatic Limits of 11 Pressure Transmitting Media. *J. Phys. D: Appl. Phys.* **2009**, *42*, 075413.

(33) Fei, Y.; Ricolleau, A.; Frank, M.; Mibe, K.; Shen, G.; Prakapenka, V. Toward an Internally Consistent Pressure Scale. *Proc. Natl. Acad. Sci. U. S. A.* **2007**, *104*, 9182−9186.

(34) Syassen, K. Ruby under Pressure. *High Pressure Res.* **2008**, *28*, 75−126.

(35) Prakapenka, V. B.; Kubo, A.; Kuznetsov, A.; Laskin, A.; Shkurikhin, O.; Dera, P.; Rivers, M. L.; Sutton, S. R. Advanced Flat Top Laser Heating System for High Pressure Research at GSECARS: Application to the Melting Behavior of Germanium. *High Pressure Res.* **2008**, *28*, 225−235.

(36) Zhang, D.; Dera, P. K.; Eng, P. J.; Stubbs, J. E.; Zhang, J. S.; Prakapenka, V. B.; Rivers, M. L. High Pressure Single Crystal Diffraction at PX 2. *J. Visualized Exp.* **2017**, No. e54660.

(37) Prescher, C.; Prakapenka, V. B. Dioptas: A Program for Reduction of Two-dimensional X-ray Diffraction Data and Data Exploration. *High Pressure Res.* **2015**, *35*, 223−230.

(38) Toby, B. H.; Von Dreele, R. B. Gsas-ii: The Genesis of a Modern Open-source All Purpose Crystallography Software Package. *J. Appl. Crystallogr.* **2013**, *46*, 544−549.

(39) DIAMOND Version 4.x, CRYSTAL IMPACT, Kreuzherrenstr. 102, 53227 Bonn, Germany.

(40) Angel, R. J.; Alvaro, M.; Gonzalez-Platas, J. EosFit7c and a Fortran Module (library) for Equation of State Calculations. *Z. Kristallogr. - Cryst. Mater.* **2014**, *229*, 405−419.

(41) Hohenberg, P.; Kohn, W. Inhomogeneous Electron Gas. *Phys. Rev.* **1964**, *136*, B864−B871.

(42) Kohn, W.; Sham, L. J. Self-consistent Equations Including Exchange and Correlation Effects. *Phys. Rev.* **1965**, *140*, A1133−A1138.

(43) Kresse, G.; Furthmüller, J. Efficiency of Ab-initio Total Energy Calculations for Metals and Semiconductors Using a Plane-wave Basis Set. *Comput. Mater. Sci.* **1996**, *6*, 15−50.

(44) Blöchl, P. E. Projector Augmented-wave Method. *Phys. Rev. B: Condens. Matter Mater. Phys.* **1994**, *50*, 17953−17979.

(45) Kresse, G.; Joubert, D. From Ultrasoft Pseudopotentials to the Projector Augmented-wave Method. *Phys. Rev. B: Condens. Matter Mater. Phys.* **1999**, *59*, 1758−1775.

(46) Perdew, J. P.; Burke, K.; Ernzerhof, M. Generalized Gradient Approximation Made Simple. *Phys. Rev. Lett.* **1996**, *77*, 3865−3868.

(47) Grimme, S. Semiempirical GGA-Type Density Functional Constructed with a Long-Range Dispersion Correction. *J. Comput. Chem.* **2006**, *27*, 1787−1799.

(48) Zhao, Y.; Truhlar, D. G. Benchmark Databases for Nonbonded Interactions and Their Use to Test Density Functional Theory. *J. Chem. Theory Comput.* **2005**, *1*, 415−432.

(49) Grimme, S.; Antony, J.; Schwabe, T.; Mück-Lichtenfeld, C. Density Functional Theory with Dispersion Corrections for Supra-molecular Structures, Aggregates, and Complexes of (Bio)Organic Molecules. *Org. Biomol. Chem.* **2007**, *5*, 741−758.

(50) Landerville, A. C.; Oleynik, I. I. Vibrational and Thermal Properties of β-HMX and TATB from Dispersion Corrected Density Functional Theory. *AIP Conf. Proc.* **2015**, *1793*, 050007.

(51) Landerville, A. C.; Conroy, M. W.; Budzevich, M. M.; Lin, Y.; White, C. T.; Oleynik, I. I. Equations of State for Energetic Materials from Density Functional Theory with van Der Waals, Thermal, and Zero-Point Energy Corrections. *Appl. Phys. Lett.* **2010**, *97*, 251908.

(52) Ernzerhof, M.; Scuseria, G. E. Assessment of the Perdew−burke−ernzerhof Exchange-correlation Functional. *J. Chem. Phys.* **1999**, *110*, 5029−5036.

(53) Tuma, C.; Boese, A. D.; Handy, N. C. Predicting the Binding Energies of H-bonded Complexes: A Comparative DFT Study. *Phys. Chem. Chem. Phys.* **1999**, *1*, 3939−3947.

(54) Santra, B.; Michaelides, A.; Scheffler, M. On the Accuracy of Density-functional Theory Exchange-Correlation Functionals for H Bonds in Small Water Clusters: Benchmarks Approaching the Complete Basis Set Limit. *J. Chem. Phys.* **2007**, *127*, 184104.

(55) Ireta, J.; Neugebauer, J.; Scheffler, M. On the Accuracy of DFT for Describing Hydrogen Bonds: Dependence on the Bond Directionality. *J. Phys. Chem. A* **2004**, *108*, 5692−5698.

(56) Novoa, J. J.; Sosa, C. Evaluation of the Density Functional Approximation on the Computation of Hydrogen Bond Interactions. *J. Phys. Chem.* **1995**, *99*, 15837−15845.

(57) Grossman, J. C.; Schwegler, E.; Draeger, E. W.; Gygi, F.; Galli, G. Towards an Assessment of the Accuracy of Density Functional Theory for First Principles Simulations of Water. *J. Chem. Phys.* **2004**, *120*, 300−311.

(58) Todorova, T.; Seitsonen, A. P.; Hutter, J.; Kuo, I.-F. W.; Mundy, C. J. Molecular Dynamics Simulation of Liquid Water: Hybrid Density Functionals. *J. Phys. Chem. B* **2006**, *110*, 3685−3691.

(59) Glass, C. W.; Oganov, A. R.; Hansen, N. USPEX-evolutionary Crystal Structure Prediction. *Comput. Phys. Commun.* **2006**, *175*, 713−720.

(60) Lyakhov, A. O.; Oganov, A. R.; Valle, M. How to Predict Very Large and Complex Crystal Structures. *Comput. Phys. Commun.* **2010**, *181*, 1623−1632.

(61) Oganov, A. R.; Glass, C. W. Crystal Structure Prediction Using Ab Initio Evolutionary Techniques: Principles and Applications. *J. Chem. Phys.* **2006**, *124*, 244704.

(62) Angel, R. New Phenomena in Minerals at High Pressures. *Phase Transitions* **1996**, *59*, 105−119.

(63) Angel, R.; Ross, N. Compression Mechanisms and Equations of State. *Philos. Trans. R. Soc., A* **1996**, *354*, 1449−1459.

(64) Chakrabborty, D.; Yash, A.; Manogaran, S. Ground State Vibrations of N-glycylglycine Hydrochloride: An Ab Initio Study. *J. Mol. Struct.: THEOCHEM* **1994**, *303*, 265−273.

(65) Christy, A. G. Isosymmetric Structural Phase Transitions: Phenomenology and Examples. *Acta Crystallogr., Sect. B: Struct. Sci.* **1995**, *51*, 753−757.

(66) Gupta, S. C.; Chidambaram, R. Symmetry Systematics of Pressure-induced Phase Transitions. *High Pressure Res.* **1994**, *12*, 51−70.

(67) Beran, G. J. O. Modeling Polymorphic Molecular Crystals with Electronic Structure Theory. *Chem. Rev.* **2016**, *116*, 5567−5613.

(68) Bardwell, D. A.; Adjiman, C. S.; Arnautova, Y. A.; Bartashevich, E.; Boerrigter, S. X.; Braun, D. E.; Cruz-Cabeza, A. J.; Day, G. M.; Della Valle, R. G.; Desiraju, G. R.; et al. Towards Crystal Structure Prediction of Complex Organic Compounds − A Report on The Fifth Blind Test. *Acta Crystallogr., Sect. B: Struct. Sci.* **2011**, *67*, 535−551.

(69) Reilly, A. M.; Cooper, R. I.; Adjiman, C. S.; Bhattacharya, S.; Boese, A. D.; Brandenburg, J. G.; Bygrave, P. J.; Bylsma, R.; Campbell, J. E.; Car, R.; et al. Report on the Sixth Blind Test of Organic Crystal Structure Prediction Methods. *Acta Crystallogr., Sect. B: Struct. Sci., Cryst. Eng. Mater.* **2016**, *72*, 439−459.

(70) Mulliken, R. S. Electronic Population Analysis on Lcao−mo Molecular Wave Functions. I. *J. Chem. Phys.* **1955**, *23*, 1833−1840.

(71) Blöchl, P. E. Electrostatic Decoupling of Periodic Images of Plane-Wave-Expanded Densities and Derived Atomic Point Charges. *J. Chem. Phys.* **1995**, *103*, 7422−7428.

(72) Silvestrelli, P. L.; Parrinello, M. Water Molecule Dipole in the Gas and in the Liquid Phase. *Phys. Rev. Lett.* **1999**, *82*, 3308−3311.